Modelling of stress evolution and its effect on formability in tension under cyclic bending plus Compression

Wenxuan Peng[1] and Hengan Ou[1*]

[1] Faculty of Engineering, University of Nottingham, Nottingham, UK, NG7 2RD
* h.ou@nottingham.ac.uk

Abstract. Single point incremental forming (SPIF) and Double-sided incremental forming (DSIF) are two main variants of incremental sheet forming (ISF) processes. Tension under cyclic bending (TCB) have been developed as a means for experimental evaluation and validation of the SPIF process and further extended to DSIF process by adding a compression force (TCBC) in recent years.
In this study, an analytical model is proposed to capture the localised deformation and stress evolutions due to bending, reverse-bending and additional compression in TCB and TCBC tests as a simplification of SPIF and DSIF processes. The results show the through-thickness stress variation has determinative influence on fracture initiation. The effects of test parameters and their interactions on formability were evaluated. Although the surface contact deformation and material thinning are simplified in the analytical model, the results obtained are comparable to experimental testing and finite element (FE) simulations. This work shows that the analytical model can be used as an effective means to decouple the complex deformation modes and local stress evolutions of TCB and TCBC and to provide a new insight into SPIF and DSIF processes.

Keywords: Bending under tension and compression, Incremental sheet forming, Modelling, Formability.

1 Introduction

Incremental sheet forming (ISF) is an emerging flexible and cost-effective sheet metal forming process. Its die-less feature and easy adaptability make it suitable for manufacturing small-batch and customised sheet parts. In addition to the common form of single point incremental forming (SPIF), double-sided incremental forming (DSIF) is a promising variant, which further enhances the formability and accuracy as compared to SPIF process. The ISF processes were extensively investigated by analytical modelling [1], forming limited curve (FLC) [2] and finite element method (FEM) [3] in previous studies. However, the limitation of direct experimental observation and measurement impedes deeper understanding of the deformation and fracture behaviour of both SPIF and DSIF processes. Tension under Cyclic Bending (TCB) and Tension under Cyclic Bending and Compression (TCBC) are considered as two representative processes to provide comparable and measurable testing methods, as illustrated in Fig. **1**a. Emmens and Boogaard [2] proposed TCB to achieve large deformation similar to

the SPIF process. In the TCB tests, the samples can achieve larger maximum strain than common tensile test, in which the pulling speed and bending depth had dominant effects on formability. Benedyk et al. [4] studied and compared in-plane strain behaviours in TCB by Circle Grid Analysis (CGA). These strain results indicated that the TCB process prolongs the stability of plastic deformation and homogenises the strain distribution in the tensile direction. Barrett et al. [5] noticed the material softening during cyclic loading and unloading and utilised a material model, which enabled a prediction of the forming force in agreement with experimental measurement.

Tension under cyclic bending and compression (TCBC) was initially introduced and researched by Ai and Long. [6]. The additional compression by a compressive roller resulted in the superior formability and the reduced tensile force, which enabled an increased forming stability for both TCBC and DSIF processes. Ai et al. [7] presented a derivation to reveal the relationship between the stresses in the tension and through-thickness directions. Peng and Ou [8] presented detailed investigations of the deformation and fracture mechanisms of TCB, TCBC and indeed the SPIF and DSIF processes in general. The results showed TCB and TCBC are comparable to SPIF and DSIF processes in terms of the cyclic deformation and stress states. However, a theoretical study to capture local stress state is absent from TCB and TCBC studies.

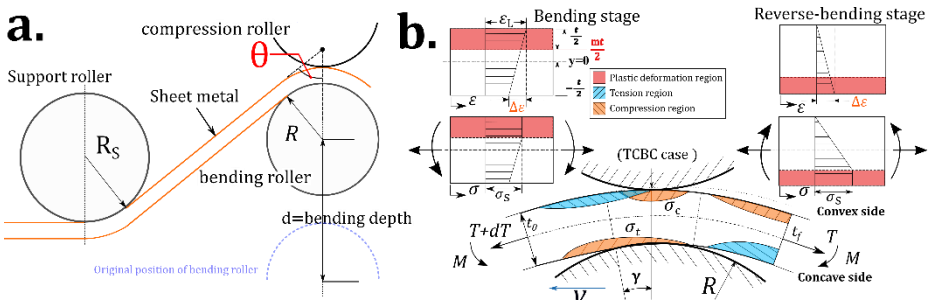

Fig. 1 Local bending for TCB and TCBC: (a) deformation regions by contact condition, and (b) strain and stress diagram for typical bending and tension process.

In this study, the analysis focuses on the regions under contact point and the through-thickness to reveal the stress and strain evolution in different forming stages. This leads to an explanation of the reduced forming forces and stress distribution, as well as a comparative assessment of key parameters to the formability using a damage function of stress triaxiality and plastic strain rate. The results are compared with the FE simulations under a unified damage criterion using accumulated products of differential stress triaxiality and plastic strain increments, which provides an insight of the correlation between the TCB, TCBC and SPIF, DSIF processes.

2 Analytical model of the TCB and TCBC tests

For simplicity, there are two basic assumptions to be made:

- The explicit stress value may not be determined as the actual contact area is difficult to measure. For convenience, the compressive stress σ_c is used in derivation.
- The material is assumed to be elastic till reaching the yield stress then being perfectly plastic.

2.1 General case of deformation

To investigate the stress state of localised deformation, Fig. **1**b shows the deformation region can be divided into two regions: region under i) bending stage and ii) reverse-bending stage. At an arbitrary time during the process, the deformation in contact region can be made up with elastic part and plastic part, separated by the surface at $y = m\frac{t}{2}$, where $m \in [-1,1]$ indicates the position of the boundary between elastic and plastic deformation regions in through-thickness direction as shown in Fig. **1**b. The material deformation is fully elastic when $m = 1$ or fully plastic when $m = -1$. Assume the yield stress in longitude direction is S, the strain at $y = m\frac{t}{2}$ can be written as:

$$\varepsilon_{y=\frac{mt}{2}} = \frac{S}{E\prime} = \frac{(1-\nu^2)S}{E} \tag{1}$$

where E' is the modulus of elasticity in plane strain condition and can be calculated by young's modulus E and Poisson's ratio ν.

Based on material rigidity, the strain distribution through-thickness is proportional to bending curvature. The through-thickness strain distribution can be presented as:

$$\varepsilon = \varepsilon_a + \Delta\varepsilon = \frac{S}{E\prime} - \frac{1}{\rho}\cdot\frac{mt}{2} + \frac{y}{\rho}\left(\rho = R + \frac{t}{2}\right) \tag{2}$$

where ε_a, ρ, R, t are the strain at central surface, distances from tool centre to central surface, tool radius and sheet thickness, respectively.

The tension distribution in radial direction can be given where S denotes the stress in the tensile direction in the yielding region $\frac{mt}{2} \le y \le \frac{t}{2}$:

$$T = \int_{-t/2}^{mt/2} E' \cdot \varepsilon dy + \int_{mt/2}^{t/2} S dy = St\left[1 - \frac{E't}{8}(m+1)^2\right] \tag{3}$$

Eq. (2) indicates a discrepancy among through-thickness strains. This strain imbalance caused by bending deformation is lowered in the reverse-bending stage where the bent material is stretched back to a straight strip (**Fig. 1**b). By force equilibrium in the thickness direction in the contact region:

$$\sigma_t \cdot 1 \cdot Rd\theta = (T + dT)\cdot sin\frac{d\theta}{2} + T \cdot sin\frac{d\theta}{2} + \kappa \cdot \sigma_c \cdot 1 \cdot (R + t)d\theta \tag{4}$$

where σ_t is the contact stress between the sample and the bending roller, σ_c is the additional compressive stress, κ is the indicator of the TCB ($\kappa = 0$) and TCBC ($\kappa = 1$) cases. Assume the higher-order terms is small enough, Eq. (4) can be reduced to:

$$\sigma_t = \frac{T}{R} + \kappa \cdot \sigma_c\left(1 + \frac{1}{R/t}\right) \tag{5}$$

Similarly, the current yield stress S can be derived with the use of Tresca's yield criterion in the plastic deformation region:

$$\sigma_Y = S + \sigma_t^{y=mt/2} \tag{6}$$

$$S = \frac{\rho+mt/2}{\rho+t/2} \cdot \sigma_Y - \kappa \cdot \sigma_c \tag{7}$$

where σ_Y is material yielding stress that can be obtained by using Johnson-Cook hardening model $\sigma_Y = A + B\varepsilon_{eq}^n$.

2.2 Strain evolution in bending and unbending process

Assume the deformation is perfectly localised that only the material under bending is deformed. As the tensile speed V_T and stroke speed V_S keeping constant during a unit time dt in the process, where the length of material being deformed is equal to the material being contacted, which is $V_S dt$. The strain increment of each tool passage ε_{incr} can be defined with V_T and V_S[2]. Because of the rigidity of material, the elongation per contact is also equal to the maximum strain increase in thickness direction:

$$\varepsilon_{incr} = \frac{V_T}{V_S}/1s = \frac{S}{E\prime} - \frac{1}{\rho} \cdot \frac{mt}{2} + \frac{t}{2\rho} \tag{8}$$

The value of elastic limit m can be solved:

$$m = 1 + \frac{2\rho S}{E't} - \frac{2V_T\rho}{V_S t} \tag{9}$$

Due to the characteristic of local bending deformation in TCB and TCBC, the elongations throughout thickness are unequal after the contact. This unbalance would be rebalanced in the following reverse-bending stage. Assume σ_L is the longitudinal stress, the stress, tension and moment distribution at a relative position of $y = \frac{pt}{2}, p \in [-1,1]$ in the thickness direction can be determined for both the bending and reverse-bending stages:

Bending stage: (10)

$$\begin{cases} \varepsilon^{y=pt/2} = \dfrac{V_T}{V_S} - \dfrac{(1-p)t}{2\rho} \\ \sigma_L = \begin{cases} E'\left(\dfrac{V_T}{V_S} - \dfrac{(1-p)t}{2\rho}\right), -1 \le p < m; \\ S, m \le p \le 1; \end{cases} \\ \sigma_t = \dfrac{\int_{pt/2}^{t/2} \sigma_L dt}{\rho + \dfrac{mt}{2}} + \kappa \cdot \sigma_c\left(1 + \dfrac{(1-p)t}{2\rho + pt}\right) \end{cases}$$

Reverse-bending stage: (11)

$$\begin{cases} \varepsilon^{y=pt/2} = (1-p)\dfrac{t}{2\rho} \\ \sigma_L = \begin{cases} (1-p)\dfrac{t}{2\rho} \cdot E', & m_{rb} < p \le 1; \\ \sigma_s, & -1 \le p \le m_{rb}; \end{cases} \\ \sigma_t = 0 \\ m_{rb} = 1 - \dfrac{2\rho\sigma_s}{E't} \end{cases}$$

The total power is the sum of bending power $\dot{W}_b$ and tension power $\dot{W}_t$ if the transfer loss is neglected. Assume M, dl are the moment and the elongation being deformed in a section, which can be given by the moving speed of tool stroke V_S as $dl = V_S dt =$

$\rho d\theta$, as well as the material being bent by incremental angle $d\theta$. Therefore, the total power $\dot{W}_{ext}$ and the increase of tension ΔT can be determined as:

$$\dot{W}_{ext} = \dot{W}_b + \dot{W}_t = \frac{Md\theta}{dt} + \frac{T\cdot\varepsilon_a dl}{dt} = V_S \cdot \left(\frac{M}{\rho} + T\cdot\varepsilon_a\right) = V_S \cdot [(T+\Delta T) - T] \quad (12)$$

$$\Delta T = \left(\frac{M}{\rho} + T\cdot\varepsilon^{y=0}\right) \quad (13)$$

Thus, the moment M and tension T in bending and reverse-bending stages can be presented as below:

At bending stage:

$$M = \int_{-\frac{t}{2}}^{\frac{mt}{2}} E'\varepsilon y dy + \int_{\frac{mt}{2}}^{\frac{t}{2}} Sy dy = \frac{t^2}{8}(m^2-1)\left(E'\left(\frac{V_T}{V_S} - \frac{t}{2\rho}\right) - S\right) + \frac{E't^3}{24}(m^3+1) \quad (14)$$

$$T = \int_{\frac{mt}{2}}^{\frac{t}{2}} S dt + \int_{-1}^{m} E'^{\left(\frac{V_T}{V_S} - \frac{(1-y)t}{2\rho}\right)} dy = \frac{St(1-m)}{2} + \frac{E'V_T}{V_S}(m+1) - \frac{E't}{2\rho}\left(m - \frac{m^2}{2} + \frac{3}{2}\right) \quad (15)$$

At reverse-bending stage:

$$M = \int_{-\frac{t}{2}}^{\frac{mt}{2}} \sigma_y y dy + \int_{\frac{mt}{2}}^{\frac{t}{2}} E'\varepsilon\cdot y dy = \frac{\sigma_y t^2(m^2-1)}{8} + \frac{E't}{2\rho}\cdot\left(\frac{t^2(1-m^2)}{8} - \frac{t^3}{24}(1-m^3)\right) \quad (16)$$

$$T = \int_{-\frac{t}{2}}^{\frac{mt}{2}} \sigma_y dt + \int_{m}^{1} \frac{(1-y)tE'}{2\rho} dy = \frac{tE'}{2\rho}\left(\frac{1}{2} - m + \frac{1}{2}m^2\right) + \frac{\sigma_y t}{2}(m+1) \quad (17)$$

At arbitrary depth in the thickness direction $y = pt/2$, The shear force F_{shear} and shear stress τ are defined:

$$F_{shear} = \Delta T \cdot \frac{\int \sigma dA}{\int_0^t \sigma dt} \quad (18)$$

$$\tau = \frac{F_{shear}Q}{Ib} = \frac{F_{shear}\int y dA}{b\int y^2 dA} = \frac{3F_{shear}(1-p^2)}{2t} \quad (19)$$

where, Q and I are the first and second moments of area, respectively. The sheet forming process can be recognised as a plane stress case where the stress in the width direction, $\sigma_w = 0$. The stress triaxiality η can be calculated and used to the equivalent damage D for estimation of material damage, suggested by Bai and Wierzbicki [9]:

$$D = \int_0^{\varepsilon} \eta d\varepsilon \quad (20)$$

Thus, the incremental damage can be accumulated by the product of the stress triaxiality and effective strain increment in each deformation stage. Thus, the effect of various stress states from compression to biaxial tension on damage in general ISF processes can be estimated and compared with. Although quantitative evaluation of failure is less tangible, the relative development of damage can be obtained and correlated to reflect the effect of process parameters, i.e. initial sheet thickness, compression stress and bending depth.

3 Results and discussion

The distributions of shear stress, stress triaxiality and damage accumulation are plotted in **Fig. 2**. The peak shear stress is reached at the neutral or middle surface where a smaller value is obtained in TCBC process (**Fig. 2**a). The overall stress triaxiality is suppressed by additional compression in TCBC as well. The stress triaxiality monotonously increases from the concave to the convex surface in the bending stage (**Fig. 2**b). However, more damage is accumulated on the concave side for all stages including the reverse-bending (**Fig. 2**c). This result suggests fracture is more likely to initiate on the concave surface of bending and the reverse-bending stage is worth more investigation in terms of its contribution to damage formation.

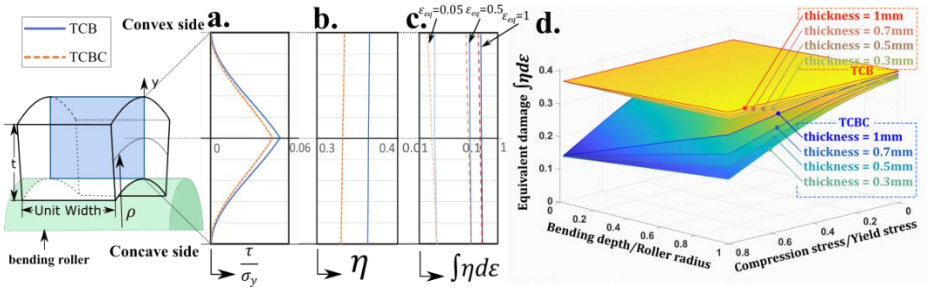

Fig. 2 Through thickness distributions of (a) normalised shear stress, (b) stress triaxiality, (c) equivalent damage by equivalent stress triaxiality in bending stage, and (d) comparison of overall equivalent damage surfaces of various thickness at equivalent strain equal to 1 in TCB and TCBC.

Fig. 2d depicts the maximum equivalent damage, defined in Eq. (20) at equivalent strain $\varepsilon_{eq} = 1$ in TCB and TCBC against the ratios of bending depth over radius, and the compression stress over material yield stress. It is evident that the impact of compression on damage reduction is substantial. The bending depth is a contributing factor to increase the damage accumulation especially in the case of TCBC. The results reveal a trend that thicker sheet mitigates compression but amplifies the impact of bending depth. Both compression and bending depth are influential factors to formability, however, the sheet thickness is a decisive factor that governs how these parameters exert the effect. Notably, larger thickness can increase the resistance to fracture in practice. Thus, proper consideration of optimizing parameters is crucial for formability.

The analytical model results are consistent with the experimental results in terms of compression and thickness, as can be referred to [8]. However, the prediction from the analytical model is less accurate to the formability changes due to bending depth. A possible reason is that the increase of bending depth has a minimal impact on the stress states but it influences more on the contact angle θ instead. The contact angle is monotonously rising with the increasing bending depth. The increasing contact angle is a positive factor for the forming stability according to Considère criterion. Hence, accurate evaluation to the effect of bending depth on formability in TCB and TCBC is limited to contact pressure estimation. This limitation may be quantified by FE simulation using a unified damage criterion as given in Eq. (20).

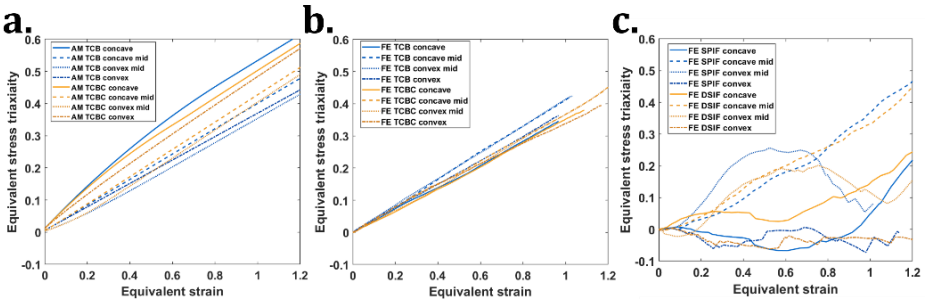

Fig. 3 Evolution of stress triaxiality against equivalent strain from (a) analytical model, (b) FE simulation of TCB and TCBC, and (c) FE simulation of SPIF and DSIF processes.

Fig. 3 presents the comparisons of the equivalent damage evolution versus strain evolution at different layers through thickness based on the analytical model and FE simulations from TCB, TCBC and SPIF, DSIF [8]. From **Fig. 3**(a) and (b), it can be observed that the TCB process displays larger through-thickness discrepancies in equivalent damage evolution when compared to the TCBC process by both the analytical model and FE simulations. The analytical model exhibited a trend to over-estimate these differences, which can be attributed to the lack of considerations of the local contact and the differential divisions of locations in the through-thickness layers. However, the equivalent stress triaxiality evolutions in SPIF and DSIF processes are not monotonically increased during the deformation process. Especially on the concave side, there is a noticeable delay of equivalent damage increase (**Fig. 3**(c)). Therefore, a comprehensive consideration of the loading processes is necessary to apply the analysis for TCB and TCBC to SPIF and DSIF processes. The cyclic bending-under-tension feature in TCB and TCBC resembles ISF processes in general. Meanwhile, the loading process in TCB and TCBC is continuous and uniform in each pass, in contrast of the discrete and localised strain evolutions, determined by the wall angle and step depth, in SPIF and DSIF, leading to variations in both the deformation and damage mechanisms.

The proposed analytical model lacks detailed capture of localised contact that prevents a precise estimation on the influence generated by the bending depth in TCB and TCBC processes. This limitation can be addressed through a quantitative investigation of the relationship between bending depth, contact angle, and pressure. In FE simulation of ISF processes, optimal mesh density requires sufficient mesh density in the tool and sheet contact region plus element layers in the through-thickness direction at the cost of computing time. Adaptive meshing may be used to achieve a balanced solution. From fracture prediction perspective, the importance of through-thickness stress and strain discrepancies to the damage evolution was highlighted. The incorporation of additional stress indicators, such as the Lode angle parameter with a new damage criterion, may enhance the ability to capture the detailed development of damage and improve the accuracy of predictions.

4 Conclusions

The proposed analytical model for TCB and TCBC processes captured the main deformation features and reveal the effect of key parameters on formability. The results are consistent with experimental results but the formability changes caused by bending depth are less accurate due to lack of consideration for local contact. This highlights the effect of through-thickness stress and strain discrepancy to the fracture initiation as well as the local contact condition. While the analytical model provides a useful analysis of the TCB and TCBC processes, it is imperative to review the effect of distinct local stress conditions and the progression of deformation leading to inhomogeneous strain rate per tool pass when applying the findings from TCB and TCBC to SPIF and DSIF processes.

References

1. Lu, B., Fang, Y., Xu, D. K., Chen, J., Ai, S., Long, H., Ou, H. & Cao, J. (2015). Investigation of material deformation mechanism in double side incremental sheet forming. International Journal of Machine Tools and Manufacture, 93, 37-48.
2. Emmens, W. C., & van den Boogaard, A. H. (2009). Incremental forming by continuous bending under tension—an experimental investigation. Journal of materials processing technology, 209(14), 5456-5463.
3. Gatea, S., Ou, H., Lu, B., & McCartney, G. (2017). Modelling of ductile fracture in single point incremental forming using a modified GTN model. Engineering Fracture Mechanics, 186, 59-79.
4. Benedyk, J. C., Kinsey, B. L., Korkolis, Y. P., & Roemer, T. J. (2015). Fundamental studies of continuous bending under tension (CBT) and potential automotive forming applications. Materials Today: Proceedings, 2(10), 4998-5005.
5. Barrett, T. J., Takagi, S., Islam, N., Kuwabara, T., Hassan, T., Kinsey, B. L., Knezevic M., & Korkolis, Y. P. (2021). Material modeling and simulation of continuous-bending-under-tension of AA6022-T4. Journal of Materials Processing Technology, 287, 116658.
6. Ai, S., & Long, H. (2019, July). Finite element modelling of material deformation and damage by tension under cyclic bending and compression test. In AIP Conference Proceedings (Vol. 2113, No. 1, p. 180012). AIP Publishing LLC.
7. Ai, S., Dai, R., & Long, H. (2020). Investigating formability enhancement in double side incremental forming by developing a new test method of tension under cyclic bending and compression. Journal of Materials Processing Technology, 275, 116349.
8. Peng, W., & Ou, H. (2023). Deformation mechanisms and fracture in tension under cyclic bending plus compression, single point and double-sided incremental sheet forming processes. International Journal of Machine Tools and Manufacture, 184, 103980.
9. Bai, Y., & Wierzbicki, T. (2008). A new model of metal plasticity and fracture with pressure and Lode dependence. International journal of plasticity, 24(6), 1071-1096.